Observation of local electronic structures of adatom vacancies in Si(111)-(7×7) surface in real space

Lan Chen, B. C. Pan, Hongjun Xiang, Bing Wang, Jinlong Yang,[*,†] J. G. Hou,[*,‡] and Qingshi Zhu
Department of Physics, Hefei National Laboratory for Physical Sciences at the Microscale, University of Science and Technology of China, Hefei, Anhui 230026, People's Republic of China
(Received 2 August 2006; revised manuscript received 28 November 2006; published 28 February 2007)

The evolution of the local electronic structure of the Si(111)-(7×7) surface containing adatom vacancies is resolved by energy-dependent scanning tunneling microscopy. The *dI/dV* images show clear and rich features that are bias dependent and can be sorted into several patterns. The probed *dI/dV* patterns reflect the different hybridized electronic features arising from the adatom vacancies. A typical electronic state associated with the single adatom vacancy in the surface is experimentally found to be at about 0.55 eV below the Fermi energy level, which is essentially attributed to the two upward backbone atoms around the adatom vacancy. We also find that adatom vacancies can induce the images of some rest atoms to be invisible in the *dI/dV* maps.

DOI: 10.1103/PhysRevB.75.085329 PACS number(s): 73.20.At, 68.37.Ef, 71.15.−m

I. INTRODUCTION

The reconstruction of the clean Si(111)-(7×7) surface at room temperature has attracted much attention because of the complexity of the surface structure. So far, the proposed dimer-adatom-stacking-fault (DAS) model[1] [shown in Fig. 1(a)] is generally accepted as a correct model for describing of the reconstructed (7×7) structure.[2–6] Each adatom spatially connects with three underlying silicon atoms in the surface, forming backbones. The local atomic structure around each adatom is distinct from the tetrahedral configuration. These strained bonds cannot stabilize the adatoms in the Si(111)-(7×7) surface very well. Some of the adatoms may displace across the surface[10] or evaporate from the surface, producing adatom vacancies there.[7–11] In essence, forming an adatom vacancy in a (7×7) unit cell will create three dangling bonds at the vacancy and annihilate one dangling bond on the removed adatom, leading to a net increment of two dangling bonds in a DAS unit cell. Such a net increment of dangling bonds in a unit cell and the structural distortion around the adatom vacancy result in a redistribution of electrons at the Si(111)-(7×7) surface. Therefore, the electronic structure of the surface should be altered to some extent.[12,13] It is worth noting that various events such as diffusion of atoms,[14] chemical adsorption of adsorbate,[15] the growth of thin films,[16] as well as the manipulation of individual adatoms[17] on the Si(111)-(7×7) surface are all subject to the adatom vacancies in the Si(111)-(7×7) surface. These events do couple with the electronic structures of the defective (7×7) surface arising from the adatom vacancies. Therefore, knowledge of the electronic structure of the adatom vacancies is fundamental to the enhancement for our understanding of the many events occurring in the Si(111)-(7×7) surface. However, the detailed electronic structures of the defective Si(111)-(7×7) surface have not adequately been investigated.[18–20]

A scanning tunneling microscope (STM) is a powerful tool for characterizing surface structures by the topographic images and probing the local electronic states at a surface by the *dI/dV* images.[21,22] In this paper, we employ a low-temperature STM to investigate the evolution of local electronic structures associated with the adatom vacancies in the Si(111)-(7×7) surface. Comparing the measured *dI/dV* images and curves with our calculated local electronic structures, we find that each single adatom vacancy in the DAS reconstruction gives rise to a sharp peak at about −0.55 eV, which can be regarded as the characteristic state of the individual adatom vacancy. More interestingly, we reveal that each adatom vacancy does induce the images of some rest atoms to be invisible in our observed *dI/dV* maps.

II. EXPERIMENT

Our experiments were conducted using an ultrahigh vacuum low-temperature scanning tunneling microscope (Omicron GmbH, SCALA). The clean Si(111) surfaces were prepared in the preparation chamber with a base pressure of 2×10^{-10} Torr by degassing the samples at 900 K for 10 h,[23,24] flashing it up to 1500 K, then rapidly cooling down to 1200 K, and slowly cooling down to room temperature. This procedure produced a reconstructed Si(111)-(7×7) surface with a low vacancy density: one defective DAS domain mostly contained one adatom vacancy. To rule out any possibility that the defects originated from some impurities, we baked out the chamber for a long time and degassed a Si(111) for about 10 h. We first prepared a nearly defect-free Si(111)-(7×7) surface by flashing the Si(111) and followed with a relatively slow cooling down process. Then, we flashed the sample again but cooled it down to room temperature a little bit faster. With this procedure, we got the defective Si(111)-(7×7) surface originating from the point vacancies rather than any impurity. The samples were transferred to the cryostat of the microscope precooled to 78 K in the STM chamber with a base pressure of 3×10^{-11} Torr. All STM measurements were performed at 78 K with a W tip that was subject to a careful cleaning treatment by Ar-ion sputtering followed by field emission. The *dI/dV* spectra were obtained by applying a modulation of a 15 mV ac signal of 2 kHz on the dc bias between the substrate-tip gap. A lock-in amplifier was used to detect the corresponding in-phase ac component in the tunneling current. The *dI/dV* im-

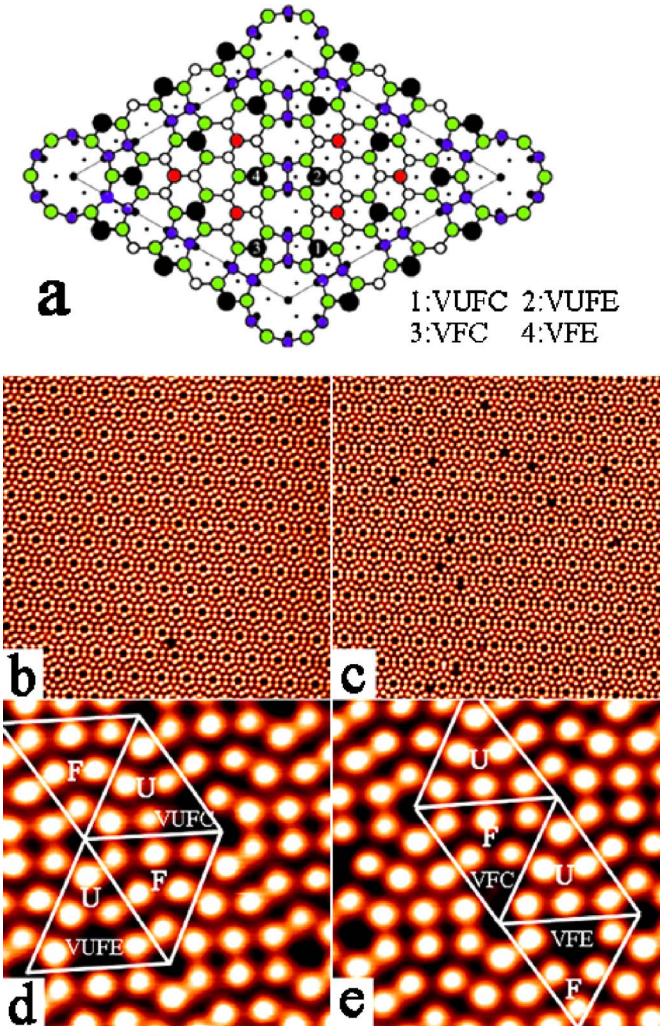

FIG. 1. (Color online) (a) Four types of adatom vacancies marked in the DAS model for the Si(111)-(7×7) surface. STM images of (b) defect-free and (c) defective Si(111)-(7×7) surface with 35×35 nm^2, measured at 1.5 V and 0.2 nA. [(d) and (e)] Magnified STM images containing four types of adatom vacancies, measured at 1.0 V and 0.4 nA. F (U) denotes the faulted (unfaulted) half unit cell. VUFC (VUFE) denotes the adatom vacancy located at unfaulted corner (unfaulted edge), and VFC (VFE) denotes the adatom vacancy located at faulted corner (faulted edge).

ages were acquired by positioning the tip of the microscope at each point at the constant current mode.

III. CALCULATION METHODS AND DETAILS

Since the measured dI/dV images are essentially correlated to the spatial distribution of local electronic states, we employed a tight-binding (TB) potential method[25] to systematically calculate the local density of states (LDOS) for the rest atoms, the adatoms, and their backbone atoms in the Si(111)-(7×7) surface. This provides a deep understanding of the origins of the measured dI/dV images. The TB potential model for silicon used in this work was developed with a correction for the bonding environment around each Si-Si bond. This potential model has been successfully employed to study the silicon clusters,[26] structural defects in bulk silicon,[27] and the silicon surface.[28,29] The accuracy and simplicity of this tight-binding potential model allows us to carry out extensive calculations for the concerned complex systems. In our calculations, the Si(111)-(7×7) surface unit cell was modeled by a slab consisting of 12 atomic layers, where periodic conditions parallel to the surface were applied. The inversion symmetry with respect to the middle of the slab was used to ensure that the two surfaces in the slab were identical. The defect-free unit cell employed in this work contained 498 Si atoms in total. We fully relaxed the selected slab model with and without an adatom vacancy, respectively, followed by calculations of the LDOS of some related atoms in the Si(111)-(7×7) surface.

IV. RESULTS AND DISCUSSION

Topologically, there are four types of adatom vacancies: a vacancy at faulted corner (VFC), faulted edge (VFE), unfaulted corner (VUFC), or unfaulted edge (VUFE) in the reconstructed (7×7) surface as shown in Fig. 1(a). These adatom vacancies were observed in our STM images, as shown in Figs. 1(b)–1(e). Figure 1(b) shows the nearly defect-free image of the Si(111)-(7×7) surface, and Fig. 1(c) shows the defective Si(111)-(7×7) surface with a low density of the defects obtained by reflashing the defect-free Si(111) but with a little faster cooling process, which indicates that the defects on the Si(111)-(7×7) surface originated from the point vacancies rather than any impurity. The magnified images in Figs. 1(d) and 1(e) give the corresponding positions of the four types of vacancies corresponding to VFC, VFE, VUFC, and VUFE in Fig. 1(a), respectively.

We recorded the scanning tunneling spectroscopy (STS) curves for these different types of vacancies in Fig. 2. For comparison, the STS curves associated with related adatoms in a defect-free surface are also given. There is a peak at around −0.3 V for the four adatoms labeled in Fig. 1(a) in the defect-free surface, in good agreement with the reported results.[4] For all the corresponding adatom vacancies, however, this peak is invisible but a new peak at −0.55 V appears. This strongly indicates that the new state is a characterizing electronic state associated with the presence of an adatom vacancy in a DAS unit cell.

In order to gain more details about its spatial distribution of the electronic structure of an adatom vacancy, we systematically measured the dI/dV maps from −1.7 to 1.7 eV with respect to the Fermi level. Figure 3 shows representative STM images and corresponding dI/dV maps at −1.0 eV for a DAS unit cell containing only one vacancy either on the faulted or on the unfaulted half. It is observed that the existence of a vacancy just affects the very half of the located vacancy but does not affect the opposite half.

Interestingly, the obtained dI/dV patterns can be roughly sorted into several groups in the considered energy range in terms of the similarity of the features in the dI/dV images. Figure 4 gives the comparison of the dI/dV maps of the different vacancies at several typical energies with those of the defect-free unit, correspondingly. In Fig. 4(a), the left diamond represents a defect-free unit, and the other triangles

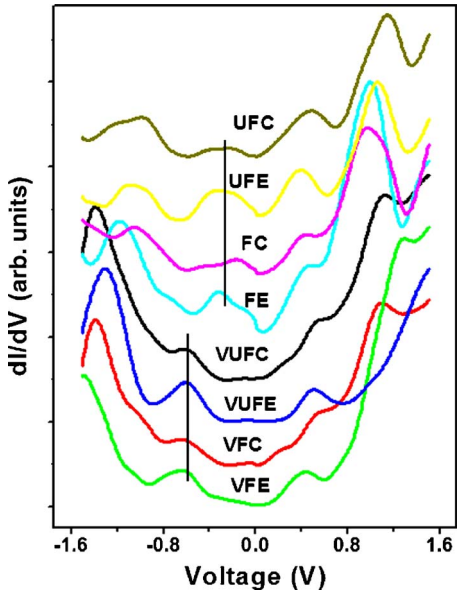

FIG. 2. (Color online) dI/dV-V curves taken over adatom vacancies and defect-free adatoms with a set point of −1.7 V and 0.4 nA. FC, FE, UFC, and UFE denote the adatom at a faulted corner, faulted edge, unfaulted corner, and unfaulted edge, respectively.

represent the faulted or unfaulted halves of the different types of vacancies. The representative dI/dV images of these adatom vacancies are displayed in Figs. 4(b)–4(g). At −0.5 eV in Fig. 4(b), it is observed that the LDOSs for some surrounding adatoms around the vacancies are brighter than those for the corresponding vacancies, which is significantly different from the nearly equal LDOS for the adatoms in the defect-free (7×7) unit. At −1.0 eV in Fig. 4(c), unlike the three triangular patterns for the rest atoms in each half in the defect-free unit, which was previously reported,[4,30] in the cases of the defective halves, one of the patterns for the rest atoms is invisible. Note that in the topographic images mentioned above, the observed vacancies in the Si(111)-(7×7) surface were adatom vacancies. We thus speculated that the

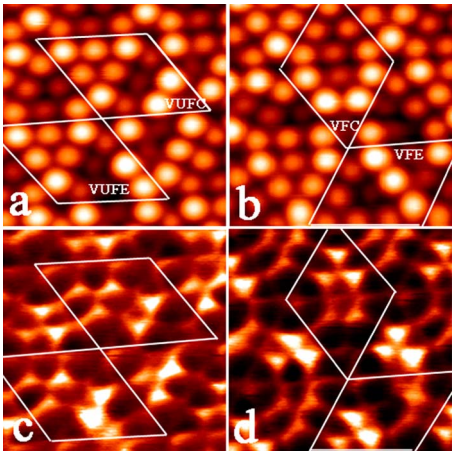

FIG. 3. (Color online) [(a) and (b)] STM images containing four types of adatom vacancies. [(c) and (d)] The corresponding dI/dV maps measured at −1.0 V and 0.4 nA.

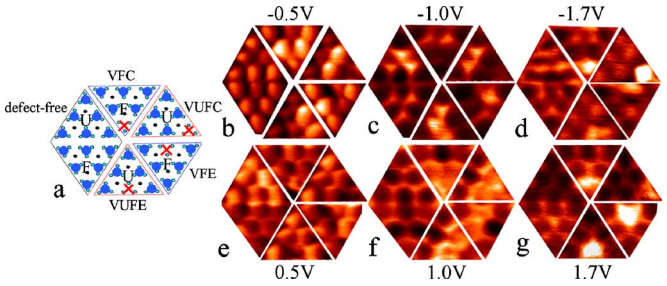

FIG. 4. (Color online) (a) Illustration of the top views of a defect-free unit cell (the left diamond) and the defective halves. The crosses denote the adatom vacancies for guiding the eyes. [(b)–(g)] dI/dV maps for comparison of the defect-free unit and the defective halves. Scanning bias is indicated in the figure.

observed missing patterns (at −1.0 eV) for the rest atoms in the defective half do not correspond to the absence of the rest atoms but still result from the adatom vacancies. However, the origination of the correlation of the adatom vacancies and the missing patterns for the rest atoms are still unclear. At −1.7 eV in Fig. 4(d), as reported before,[4] the weak dI/dV pattern in the defect-free unit mainly reflects the contributions of the electronic states of the backbone atoms; however, the dI/dV patterns in defected halves give unusually high LDOSs at the sites of adatom vacancies. We believe these high LDOSs at the vacancies should also be associated with the local electronic structures around the vacancies.[18,20]

The dI/dV patterns around the vacancies of the unoccupied states shown in Figs. 4(e)–4(g) are all distinct from those in the defect-free Si(111)-(7×7) surface. However, the patterns featuring extended brighter patterns around the vacancies are much more intricate. The intricacy stems from the information of the geometric structure as well as the related electronic structure. The geometric structure can be regarded as a constant factor for the images of dI/dV at various bias voltages, while the electronic structure at different energies exhibiting different hybridizations is the main factor causing the complexity in the dI/dV patterns.[21,22]

To have a comprehensive understanding of the experimental observations, we have to consider the electronic structure of the defective Si(111)-(7×7) surfaces. The calculated LDOSs are plotted in Fig. 5. First of all, the main features in the calculated LDOSs in Figs. 5(b1), 5(c1), 5(d1), and 5(e1) of adatoms in the defective Si(111)-(7×7) surface are quite similar to that in Fig. 5(a1) of the adatoms in a defect-free Si(111)-(7×7) surface. The adatoms in the defective DAS surface do also largely contribute to the electronic density of states at the Fermi level. These aspects mean that any adatom vacancy could not alter the electronic structures of adatoms in the defective DAS surface effectively.

However, the presence of an adatom vacancy in a DAS unit cell significantly induces the changes in the LDOS of the rest atoms. From our calculations, the LDOS in Fig. 5(a2) of the rest atoms in the defect-free DAS surface clearly shown two sharp peaks at −0.8 and −0.7 eV, which mainly correspond to the rest atoms located at the unfaulted and faulted domains, respectively. When an adatom vacancy is present at either a faulted corner (VFC) or an unfaulted cor-

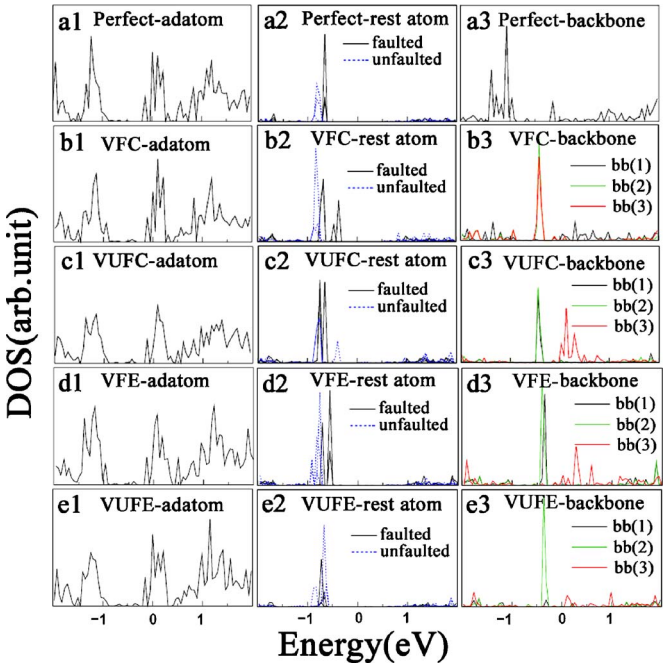

FIG. 5. (Color online) Calculated LDOSs of related adatoms, rest atoms, and backbone atoms for (a) the defect-free surface and for [(b)–(e)] the defective Si(111)-(7×7) surface. The Fermi levels are at zero. The bb(1), bb(2), and bb(3) in (b3)–(e3) stand for the three backbone atoms at each adatom vacancy.

ner (UVFC) site in a DAS unit cell, the main peaks in the LDOS of the rest atom nearest to the vacancy shift by about 0.3 and 0.4 eV, with respect to the peaks shown in Fig. 5(a2) for the rest atoms in the defect-free Si(111)-(7×7) surface, toward the Fermi energy level for the case of VFC and the case of VUFC, respectively, as shown in Figs. 5(b2) and 5(c2). This provides evidence that the rest atom nearest to the vacancy does not contribute to the LDOS at −0.7 eV in the case of a vacancy at a corner site. Therefore, the sharp peak at around −0.7 eV in the LDOS for the case of the defected corner predominantly originates from the other two rest atoms in the defective half of the DAS unit cell and the three rest atoms in the defect-free half of the DAS unit cell. As a consequence, the LDOS peaks at −0.7 eV mainly contain information from the five rest atoms. This is fully consistent with our measured dI/dV image in Figs. 3 and 4(c), where five brighter spots exist corresponding to the five rest atoms in a DAS unit cell with adatom vacancy at either a faulted or an unfaulted corner site.

In the case of adatom vacancies at either a faulted edge or an unfaulted edge, the calculated LDOSs of the rest atoms show weakly split features, where the LDOS at around −0.7 eV for the case of vacancy at an edge site is mainly associated with two rest atoms in the defective half of the unit cell and three rest atoms in the defect-free half of the unit cell. It is noted that there are two rest atoms nearest to an adatom at an edge site in the defect-free DAS unit cell. Our calculation reveals that the generated adatom vacancy at an edge site in a DAS unit cell causes one of the two rest atoms nearest to this vacancy to make no contribution to the LDOS at almost around −0.7 eV. So, the components in the concerned LDOS are mainly from the other two rest atoms in the defective domain and the three rest atoms in the defect-free domain in a DAS unit cell. This is quite different from the case of an adatom vacancy located at any corner site as mentioned above.

Usually, the electronic structure couples with the local structural features in the system. We, therefore, pay attention to the structure of the six rest atoms in the Si(111)-(7×7) surface containing an adatom vacancy. In the case of an adatom vacancy present in a DAS unit cell, the locations of three rest atoms in the defect-free domain are almost unchanged, but one of the three rest atoms in the defected domain are shifted downward toward the surface with respect to the original positions in the defect-free DAS unit cell. Thus, the original local symmetry of C_{3v} in a defect-free domain in a DAS unit cell is broken, leading to the nonequivalence of the three rest atoms in the defected domain. Mulliken charge analysis indicates that the downward rest atom gains more electron charge than the other two in the defected DAS unit cell. The aspects in the local structures and the redistribution of electron charges for the concerned rest atoms effectively result in the local electronic states of the concerned rest atoms to be degenerate. Very interestingly, our calculation reveals that it is the two upward rest atoms in each defected domain that contribute to the peaks at around −0.7 eV in the LDOS shown in Figs. 5(b2)–(e2). This is in excellent agreement with the observed dI/dV images shown in Fig. 4(c). We emphasize that all of the obtained results above originate from the existed adatom vacancy. Therefore, we can conclude that the dark spot at the location of the rest atom in each defective unit cell shown in Fig. 4(c) does not imply a missing rest atom but is actually subject to the presence of the related single adatom vacancy in a (7×7) unit cell.

Structurally, removal of an adatom from a DAS unit cell not only causes the structural distortion between the rest atoms as mentioned above but alters the local geometry around the adatom vacancy as well. Structural examination shows that two backbone atoms around a vacancy move upward and the third moves downward with respect to their original positions. In the mean time, the dangling bonds at these backbone atoms could not rebond to each other. Hence, the three dangling bonds in each adatom vacancy remain there. Commonly, these dangling bonds generate new electronic states near the Fermi energy level. Our calculations indeed reveal new sharp peaks at about 0.5 eV below the Fermi energy level and smaller peaks at around 0.3 eV above the Fermi energy level in the LDOS of the backbone atoms for the four defected cases [Figs. 5(b3)–(e3)]. To go further, we find that the former corresponds to the two upward backbone atoms and the latter to the downward backbone atom for each considered case. The Mulliken charge analysis indicates that the two upward backbone atoms gain more electronic charge, and the downward backbone atom loses electronic charge as compared to those in defect-free case. These backbone atoms mainly result in the unusual brighter spots around the adatom vacancies shown in Fig. 4(b) and the additional peak at −0.55 V in Fig. 2.

Let us further pay attention to another aspect shown in the evolution of the local electronic states in Fig. 4. It is ob-

served from Fig. 4 that the closer the electronic states are to the Fermi level, the more localized the spots in the patterns are. Otherwise, the patterns are extended. Our calculated partial LDOSs indicate that the $3s$ and $3p_z$ orbitals of the silicon atoms predominately contribute to the LDOS near the Fermi level, whereas the other electronic states are hybridized by the $3s$, $3p_x$, $3p_y$, and $3p_z$ orbitals. Spatially, the cross sections of both $3s$ and $3p_z$ orbitals in a plane parallel to the surface unit cell are in a localized shape of circle spots. In contrast, the cross sections of the $3p_x$ and $3p_y$ orbitals show more extended patterns within the same plane than those of the $3s$ and $3p_z$ orbitals. This is the reason that the probed patterns of the local electronic states near the Fermi level are to be localized while the others are much extended.

V. CONCLUSION

In summary, the local electronic structures of the Si(111)-(7×7) surface containing adatom vacancies were mapped out using energy-dependent low-temperature STM. We not only experimentally provide the evolution of local electronic states of the defective DAS reconstruction upon the discrete eigenstates but also reveal that the typical electronic states at about -0.5 eV are associated with the single adatom vacancies. Furthermore, we find that these states are originated from the upward backbone atoms in each vacancy. In addition, combining with our theoretical analysis, we demonstrate that the measured dark images located at the rest atoms in the defective domains do not correspond to the absence of the rest atoms but are caused by the existing adatom vacancies.

ACKNOWLEDGMENTS

This work was supported by the National Basic Research Program of China (2006CB0L12), by the National Natural Science Foundation of China (50121202, 50532040, 10374083, and 20573099), by the USTC-HP HPC project, and by the Virtual Laboratory for Computational Chemistry of CNIC and Supercomputing Center of CNIC, Chinese Academy of Sciences.

*Authors to whom correspondence should be addressed.
†Electronic address: jlyang@ustc.edu.cn
‡Electronic address: jghou@ustc.edu.cn

[1] K. Takayanagi, Y. Tanishiro, M. Takahashi, and S. Takahashi, J. Vac. Sci. Technol. A **3**, 1502 (1985).
[2] J. E. Northrup, Phys. Rev. Lett. **57**, 154 (1986).
[3] G.-X. Qian and D. J. Chadi, Phys. Rev. B **35**, 1288 (1987).
[4] R. J. Hamers, R. M. Tromp, and J. E. Demuth, Phys. Rev. Lett. **56**, 1972 (1986); R. Wolkow and Ph. Avouris, *ibid.* **60**, 1049 (1988).
[5] E. Bengu, R. Plass, L. D. Marks, T. Ichihashi, P. M. Ajayan, and S. Iijima, Phys. Rev. Lett. **77**, 4226 (1996).
[6] I. Stich, M. C. Payne, R. D. King-Smith, J-S. Lin, and L. J. Clarke, Phys. Rev. Lett. **68**, 1351 (1992).
[7] T. T. Tsong, R. L. Lo, T. C. Chang, and C. Chen, Surf. Rev. Lett. **1**, 197 (1994).
[8] R. S. Becker, J. A. Golovchenko, D. R. Hamann, and B. S. Swartzentruber, Phys. Rev. Lett. **55**, 2032 (1985).
[9] J. Kanasaki, T. Ishida, K. Ishikawa, and K. Tanimura, Phys. Rev. Lett. **80**, 4080 (1998).
[10] B. C. Stipe, M. A. Rezaei, and W. Ho, Phys. Rev. Lett. **79**, 4397 (1997).
[11] H. Uchida, D. Huang, F. Grey, and M. Aono, Phys. Rev. Lett. **70**, 2040 (1993).
[12] H. Lim, K. Cho, R. B. Capaz, J. D. Joannopoulos, K. D. Brommer, and B. E. Larson, Phys. Rev. B **53**, 15421 (1996).
[13] G. Treboux, T. Nakayama, H. Uchida, and M. Aono, J. Phys. Chem. B **101**, 9570 (1997).
[14] K. Wang, C. Zhang, M. M. T. Loy, and X. Xiao, Phys. Rev. Lett. **94**, 036103 (2005).
[15] C. Zhang, G. Chen, K. Wang, H. Yang, T. Su, C. T. Chan, M. M. T. Loy, and X. Xiao, Phys. Rev. Lett. **94**, 176104 (2005); Y. L. Wang, H.-J. Gao, H. M. Guo, S. W. Wang, and S. T. Pantelides, *ibid.* **94**, 106101 (2005).
[16] M. H. Upton, C. M. Wei, M. Y. Chou, T. Miller, and T.-C. Chiang, Phys. Rev. Lett. **93**, 026802 (2004).
[17] P. A. Soloan and R. E. Palmer, Nature (London) **434**, 367 (2005).
[18] Y. Utsugi, S. Yamanaka, and T. Nagamura, Appl. Phys. A: Mater. Sci. Process. **72**, S213 (2001).
[19] T. Yamauchi, Y. Takahara, and N. Narita, J. Jpn. Inst. Met. **68**, 904 (2004).
[20] T. Yamauchi, Y. Takahara, and N. Narita, Mater. Trans. **46**, 716 (2005).
[21] K. D. Wang, J. Zhao, S. F. Yang, L. Chen, Q. X. Li, B. Wang, S. H. Yang, J. L. Yang, J. G. Hou, and Q. S. Zhu, Phys. Rev. Lett. **91**, 185504 (2003).
[22] L. Chen, H. J. Xiang, B. Li, A. D. Zhao, X. D. Xiao, J. L. Yang, J. G. Hou, and Q. S. Zhu, Phys. Rev. B **70**, 245431 (2004).
[23] J. G. Hou, Jinlong Yang, Haiqian Wang, Qunxiang Li, Changgan Zeng, Hai Lin, Wang Birg, D. M. Chen, and Qingshi Zhu, Phys. Rev. Lett. **83**, 3001 (1999).
[24] H. Q. Wang, C. G. Zeng, Q. X. Li, B. Wang, J. L. Yang, J. G. Hou, and Q. S. Zhu, Surf. Sci. **442**, L1024 (1999).
[25] C. Z. Wang, B. C. Pan, and K. M. Ho, J. Phys.: Condens. Matter **11**, 2043 (1999).
[26] K. M. Ho, A. A. Shvartsburg, B. C. Pan, Z. Y. Lu, C. Z. Wang, J. G. Wacker, J. L. Fye, and M. F. Jarrold, Nature (London) **392**, 582 (1998).
[27] J. R. Morris, Z. Y. Lu, D. M. Ring, J. B. Xiang, K. M. Ho, C. Z. Wang, and C. L. Fu, Phys. Rev. B **58**, 11241 (1998).
[28] C. Z. Wang, B. C. Pan, J. B. Xiang, and K. M. Ho, Surf. Sci. **436**, L697 (1999).
[29] B. C. Pan, Surf. Sci. **599**, 85 (2005).
[30] R. I. Uhrberg, T. Kaurila, and Y.-C. Chao, Phys. Rev. B **58**, R1730 (1998).